JACS
JOURNAL OF THE AMERICAN CHEMICAL SOCIETY
Article
pubs.acs.org/JACS

Influence of Lattice Polarizability on the Ionic Conductivity in the Lithium Superionic Argyrodites Li_6PS_5X (X = Cl, Br, I)

Marvin A. Kraft,[†] Sean P. Culver,[†] Mario Calderon,[∥] Felix Böcher,[†] Thorben Krauskopf,[†] Anatoliy Senyshyn,[§] Christian Dietrich,[†,‡] Alexandra Zevalkink,[∥] Jürgen Janek,[†,‡] and Wolfgang G. Zeier*[,†,‡]

[†]Institute of Physical Chemistry, Justus-Liebig-University Giessen, Heinrich-Buff-Ring 17, D-35392 Giessen, Germany
[‡]Center for Materials Research (LaMa), Justus-Liebig-University Giessen, Heinrich-Buff-Ring 16, D-35392 Giessen, Germany
[§]Heinz Maier-Leibnitz Zentrum, Technische Universität München, 85748 Garching, Germany
[∥]Chemical Engineering and Materials Science, Michigan State University, East Lansing, Michigan 48109, United States

Supporting Information

ABSTRACT: In the search for novel solid electrolytes for solid-state batteries, thiophosphate ionic conductors have been in recent focus owing to their high ionic conductivities, which are believed to stem from a softer, more polarizable anion framework. Inspired by the oft-cited connection between a soft anion lattice and ionic transport, this work aims to provide evidence on how changing the polarizability of the anion sublattice in one structure affects ionic transport. Here, we systematically alter the anion framework polarizability of the superionic argyrodites Li_6PS_5X by controlling the fractional occupancy of the halide anions (X = Cl, Br, I). Ultrasonic speed of sound measurements are used to quantify the variation in the lattice stiffness and Debye frequencies. In combination with electrochemical impedance spectroscopy and neutron diffraction, these results show that the lattice softness has a striking influence on the ionic transport: the softer bonds lower the activation barrier and simultaneously decrease the prefactor of the moving ion. Due to the contradicting influence of these parameters on ionic conductivity, we find that it is necessary to tailor the lattice stiffness of materials in order to obtain an optimum ionic conductivity.

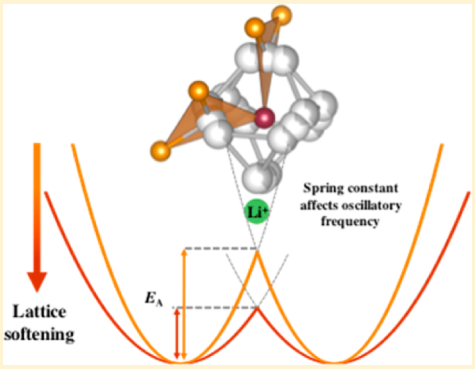

1. INTRODUCTION

Solid ion conductors (solid electrolytes) with high ionic conductivities are indispensable in many applications, such as batteries,[1−3] solid oxide fuel cells,[4] solar thermal generators,[5] and oxygen sensors.[4,6] Importantly, ionic conductivities of solid electrolytes are strongly related to their underlying crystal structure. The ionic conductivity (σ) of solids can be described by an activated hopping process of ions from one lattice site to an empty adjacent lattice site, governed by the activation barrier for the jump (E_A), the mobility (μ), the active carrier density (n), and the charge of the ion (Ze):

$$\sigma = nZe\mu \quad \text{and} \quad \mu \propto \exp\left(\frac{-E_A}{k_B T}\right) \tag{1}$$

In general, certain static structural conditions must be satisfied in order for significant ionic conductivity to occur in a solid: (1) Carrier density and available lattice sites are needed. The conductivity depends on the carrier concentration, and a large number of mobile ions must be present in the solid. Moreover, unoccupied adjacent crystallographic sites must be available for mobile ions to jump to.[6−8] Thus, solids with ionic conductivities resulting primarily from (point) defects usually exhibit lower conductivities in comparison to superionic conductors, in which a much larger number of possible crystallographic sites are occupied by the diffusing species.[6,7] For instance, α-AgI,[6] $(Ag/Cu)_7PSe_6$,[9,10] and the Li^+ conducting garnets $Li_5La_3Ta_2O_{12}$,[11,12] possess ion distributions over a large number of crystallographic sites and exhibit high ionic conductivities, even at room temperature. (2) Low activation energy is also required. While a large number of empty sites is paramount for the diffusion of ions, these sites need to be easily accessible as well. The different sites should ideally have similar potential energies with low energetic barriers for jumps between adjacent sites. The close proximity of lattice sites and favorable ion mobility can be achieved in materials with face-sharing polyhedra, as opposed to edge-sharing, since the opening (i.e., window of the diffusion pathway) in the face-shared case is larger.[7,13] Additionally, these broad diffusion pathways should be structured such that the diffusing ion does not disrupt the local arrangement of neighboring ions within the lattice.[14−16] The effects of polyhedral connectivity on the

Received: June 22, 2017
Published: July 25, 2017

DOI: 10.1021/jacs.7b06327
J. Am. Chem. Soc. 2017, 139, 10909−10918

ionic conductivity have been shown previously, for instance, in garnet-type solid electrolytes.[17]

In addition to these more static structural parameters, a larger polarizability of the anions in the same structure allows for similar hopping-site environments and has been suggested to lower the activation barriers.[15] A large number of sulfide, thiophosphate, and iodide materials are said to be superionic conductors for this reason (e.g., $Li_{10}(Sn/Ge)P_2S_{12}$, thio-LISICON Li_4GeS_4, and the above-mentioned α-AgI).[6,7,18−24] Although high ionic conductivity implies relatively weak effective coupling between mobile ions and the fixed lattice,[7] lattice−cation interactions are not negligible.

During the 1970s/1980s, several researchers put forward the idea of exploring the dynamics of the host lattice instead of focusing on the static properties.[22,25−28] For instance, the ionic conductivity should be closely related to the phonon spectrum, given that ionic diffusion is a thermally activated process.[29] The phonon spectrum resulting from lattice vibrations directly correlates to the elastic stiffness or softness of the lattice. Fischer et al. reported the importance of covalency and anion overlap in silver halides.[30] Moreover, Zeller et al. have shown the influence of anion polarizability on the oscillator strength of the lattice and, consequently, the transition rate of the hopping ion.[22,31] This in turn correlates well with ionic transition state theory that relates the prefactor of ionic motion to the Debye frequency of the lattice.[32] However, the majority of such research efforts have focused on the lattice dynamics of individual superionic conductors like α-AgI as characterized by inelastic neutron scattering.[30,33−35] Further, there have been suggestions of the influence of soft phonon modes on superionic phase transitions, but not the diffusion process per se.[36,37] No attempts have been made to systematically alter the dynamics of the host lattice of different materials and understand its influence on ionic conduction. Recent studies have only hinted at the role of lattice dynamics on specific properties. For instance, it has been shown that compositional changes in ceria lead to softer lattice vibrations, expressed as a decrease of the phonon density of states.[38] Theoretical results by Benedek et al. suggest a "phonon-assisted diffusion mechanism" via octahedral rotations in O^{2-}-conducting Ruddlesden−Popper phases.[39] Similarly, the so-called "paddle-wheel mechanism" discussed by Jansen,[40] suggests that the anions act like a revolving door, helping the cations to move through the lattice. A recent work highlighted the influence of the phonon frequency on the activation barrier, corroborating that a softer lattice and lower phonon frequencies lead to a reduction in the associated activation barriers.[41]

However, historically, it has been difficult to probe the influence of a dynamic lattice on a specific property. Inspired by the existing, but not fully understood, relationship of a soft and dynamic lattice on the ionic conductivity, we aim to provide evidence on how changing the polarizability of the anion sublattice in one structure affects the ionic transport. In this work, we employ the argyrodite Li_6PS_5X as a model system in which the halide content, and, hence, the polarizability of the anion framework, can be altered without major changes to the structure or the Li^+ diffusion pathways. By combining structural characterization with speed of sound measurements to obtain information about the materials softness and electrochemical impedance spectroscopy, we show that the lattice softness has a strong influence on the ionic transport. The presented work corroborates that a softer lattice lowers the activation barrier for a jump. However, a softer lattice also decreases the attempt frequency of the jump and the entropy of migration, precisely because of a reduction of the average vibrational frequencies of the lattice. The simultaneous decrease in the attempt frequency, entropy of migration, and activation barrier have contradicting influences on the ionic conductivity. This work is a stepping stone to gain a better understanding of the influence of a dynamic lattice on ionic transport. It highlights the importance of tailoring the lattice stiffness and suggests a necessary paradigm shift regarding the knowledge that a soft lattice is not necessarily always better for a solid ionic conductor.

2. EXPERIMENTAL METHODS

Synthesis. All preparations and sample treatments for Li_6PS_5X (X = Cl, $Cl_{0.25}Br_{0.75}$, $Cl_{0.5}Br_{0.5}$, $Cl_{0.75}Br_{0.25}$, Br, $Br_{0.75}I_{0.25}$, $Br_{0.5}I_{0.5}$, $Br_{0.25}I_{0.75}$, and I) were carried out under argon atmosphere. Lithium sulfide (Li_2S, Sigma-Aldrich, 99.98%), phosphorus pentasulfide (P_2S_5, Sigma-Aldrich, 99%), as well as LiCl (ChemPur, 99.99%), LiBr (ChemPur, 99.995%), and LiI (Alpha Aesar, 99.995%) were mixed in the appropriate stoichiometric ratio. All mixtures were hand ground in an agate mortar, pressed into pellets, and then filled into quartz ampules (10 mm inner diameter and 10−12 cm in length), which were sealed under vacuum. All ampules were carbon-coated and preheated at 800 °C under dynamic vacuum to avoid all traces of water in the reaction atmosphere. The reactions were performed at 550 °C for 2 weeks in order to ensure a complete reaction and phase purity. The obtained mixture was subsequently ground and isostatically pressed into pellets (10 mm diameter) for the electrochemical and speed of sound measurements or kept as a powder for the diffraction studies. In order to obtain standard deviations on each data set, reflecting changes in microstructure and small compositional changes, each composition was synthesized multiple times. Three syntheses per composition were used for each of the speed of sound, impedance spectroscopy, and neutron diffraction measurements.

Neutron Powder Diffraction. High-resolution neutron powder diffraction data collection on the argyrodite samples was performed in a Debye−Scherrer geometry at the Heinz Maier-Leibnitz Zentrum (research reactor FRM II, Garching b. München, Germany) on the high-resolution diffractometer SPODI.[42] Data collection using one wavelength was performed, i.e., monochromatic neutrons [λ = 1.548 17(2) Å], and were obtained from the thermal neutron beam at a 155° takeoff angle using the 551 and 331 reflections of a vertically focused composite Ge monochromator of 200 mm height. The vertical position-sensitive multidetector (300 mm vertical sensitivity range at 1.117 m sample-to-detector distance) consisting of 80 ^{3}He tubes and covering an angular range of 160° 2θ was used for data collection. The samples (approximately 2 cm^3 in volume) were filled into a thin-walled (0.15 mm) vanadium can 12 mm in diameter under argon atmosphere and then metal-sealed using indium wire. The vanadium container was then mounted on a capillary spinner enabling sample rotation, thus minimizing the effects of preferred crystallite orientations. Two-dimensional powder diffraction data of the continuously rotated sample were collected and corrected for geometrical aberrations and detector nonlinearities.[43]

Rietveld Analysis. Rietveld refinements were carried out using GSAS II software.[44] The peak profile shape was described by a pseudo-Voigt function using the modified Thomson−Cox−Hastings setting. The instrumental resolution was determined using $Na_2Ca_3Al_2F_{14}$ as the reference material. Fit indicators—R_{wp}, R_{exp}, and χ^2—were used to assess the quality of the refined structural models.[45] The following parameters were initially refined: (1) scale factor, (2) background coefficients using a Chebyschev function with 10 free parameters, (3) peak shape, which was modeled using a modified Thomson−Cox−Hastings pseudo-Voigt function,[46] (4) lattice constants, (5) fractional atomic coordinates, (6) isotropic atomic displacement parameters, and (7) zero-shift error. Finally, (8) atomic occupancies of the anions were then allowed to refine simultaneously with all other parameters, to quantify the anion site disorder.

DOI: 10.1021/jacs.7b06327
J. Am. Chem. Soc. 2017, 139, 10909−10918

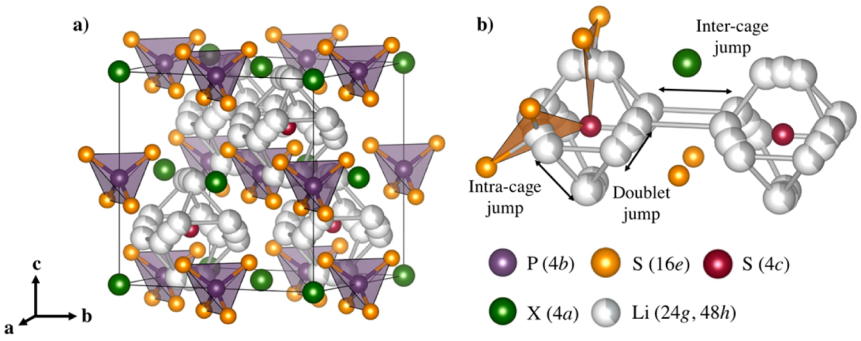

Figure 1. (a) Crystal structures of Li_6PS_5X with X = Cl, Br, I. In the ordered structure, X^- anions form a cubic close-packed lattice with PS_4^{3-} tetrahedra in the octahedral sites and the free S^{2-} (Wyckoff 4c) in half of the tetrahedral holes. (b) The free S^{2-} anions and the corner of the PS_4^{3-} tetrahedra form Frank−Kasper polyhedra, which enclose two different Li positions. The Li positions form localized cages in which multiple jump processes are possible. Jumps between the lithium positions (48*h*−24*g*−48*h*, doublet jump), intracage jumps (48*h*−48*h*), and intercage jumps can occur. The intercage jumps are suggested to dominate long-range transport, and site disorder between the 4*a* and 4*c* sites is known to affect the conductivity significantly.[64]

Synchrotron Pair Distribution Function Analysis. Mark-tubes made of borosilicate glass (Hilgenberg) with an outer diameter of 0.9 mm were filled in an argon glovebox and flame-sealed. X-ray scattering data suitable for pair distribution function and diffraction analysis were performed at room temperature using the I15 instrument at the Diamond Light Source (UK) beamline. High-energy X-rays (λ = 0.173 369 Å, 71.52 keV, bent Laue monochromator) were used in combination with a PerkinElmer 1621 EN area detector.

The crystallographic data, obtained from the refinements of the Bragg data, were used as starting values for the analysis of the PDF data of Li_6PS_5X (X = Cl, $Cl_{0.5}Br_{0.5}$, Br, $Br_{0.5}I_{0.5}$, and I). The pair distribution function [$G(r)$] was employed for a more accurate structural analysis, and the PDFgetX2 software was used to extract $G(r)$ from the raw diffraction data.[47] The collected data were first corrected for background, sample absorption, and Compton scattering. Then, normalized structure functions [$S(Q)$] were obtained. Finally, $S(Q)$ was Fourier-transformed to yield $G(r)$. A maximum scattering vector (Q_{max}) of 17 $Å^{-1}$ was employed in the Fourier transform. Structural refinements were carried out using the PDFgui software.[48] The local crystal structure of the Li_6PS_5X crystallites was refined in the $F\bar{4}3m$ space group. The fit of this structural model to the experimental PDF data was performed in the 1.8−30 Å interatomic distance range. The following parameters were refined: (1) scale factor, (2) lattice parameters (a), (3) local correlated motion factor, (4) fractional atomic coordinates of the sulfur atoms, and (5) atomic isotropic displacement parameters. Fractional atomic coordinates for the lithium atoms were fixed to values determined from the refinement of neutron diffraction data, and atomic displacement parameters for the lithium atoms were fixed to U_{iso} = 0.05. The R_w indicator was employed to assess the quality of the refined structural models.[49]

Electrochemical Impedance Spectroscopy. Electrical conductivities were measured by ac impedance spectroscopy, using a custom-built setup. Powder samples were placed between two stainless steel rods with 10 mm diameter and pressed at 3 tons for 3 min. Electrochemical impedance analysis (EIS) was conducted in the temperature range from −10 to 60 °C using a SP300 impedance analyzer (Biologic) at frequencies from 7 MHz to 100 mHz with an amplitude of 10 mV. For the samples analyzed here, all compositions have been synthesized and characterized three times in order to obtain standard deviations and reflect changes in composition and microstructure. All values shown reflect the average values and the corresponding standard deviations.

Ultrasonic Speed of Sound Measurements. Pulse-echo speed of sound measurements were performed on consolidated disks using an Epoch 600 (Olympus) with 5 MHz transducers for longitudinal and transverse speeds of sound. Since the samples are highly air sensitive and enclosing the pellets in pouches would prevent penetration of transverse signals, the samples were coated with a thin layer (<200 nm) of gold in order to prevent side reactions of the couplant and the sample. All measurements were performed under a nitrogen atmosphere. The measurement uncertainty from the speed of sound data results stems from the uncertainty in the thickness and the porosity. As the measurement uncertainty for the thickness of the pellet is much higher than that of the gold layer, the thin layer of Au is not expected to add significantly to the measurement uncertainty. In addition, no damping of the signal is expected due to the high crystallinity and high speed of sound in Au. This measurement procedure has recently been shown to be successful in understanding the lattice softness of $Li_{10}GeP_2S_{12}$.[50] While in typical sound measurements on 100% dense samples an uncertainty of 2% can be achieved, here each sample composition has been synthesized and measured three times in order to obtain standard deviations on these 85% dense samples. All values shown reflect the average values with the corresponding standard deviations.

Resonant ultrasound spectroscopy (RUS) measurements were performed on an additional set of samples (two samples of each composition) using a commercial RUSpec system built by Quasar International.[51,52] Measurements were carried out in an argon-filled glovebox to avoid sample decomposition. In contrast to the pulse-echo method, RUS measurements do not require a couplant fluid for signal transmission, so no Au film was required. A drive transducer sweeps across a frequency range of 30−350 kHz, and two pickup transducers record peaks whenever a resonant frequency of the sample is reached. The elastic tensor elements C_{11}, C_{12}, and C_{44} were determined from the RUS spectra using commercial software (RPModel, Quasar International). For each scan, the overall goodness-of-fit, as characterized by the root-mean-square (rms) difference between the predicted and observed resonant frequencies, was less than 0.5%. The speeds of sound were calculated from the elastic constants using $v_{trans} = \sqrt{C_{44}/d}$ and $v_{long} = \sqrt{(C_{11} + 2C_{12} + 4C_{44})/(3d)}$, where d is the geometrically determined density of the samples.[53]

Ultrasonic measurements are a widely used and extremely accurate approach to determine the elastic properties and speed of sound in materials.[52,53] Such methods are a direct probe of the strength of the bonds themselves.[54−57] Further, the obtained longitudinal and transverse speeds of sound (v_{long} and v_{trans}) can be used to calculate the mean speed of sound (v_{mean}), as well as the Debye temperature (Θ_D) and Debye frequency (υ_D) via eqs 2−4.[58−60]

$$v_{mean}^{\ 3} = \frac{3}{v_{long}^{\ -3} + 2v_{trans}^{\ -3}} \tag{2}$$

$$\Theta_D = \frac{\hbar}{k_B}\left(\frac{6\pi^2}{V}\right)^{1/3} v_{mean} \tag{3}$$

DOI: 10.1021/jacs.7b06327
J. Am. Chem. Soc. 2017, 139, 10909−10918

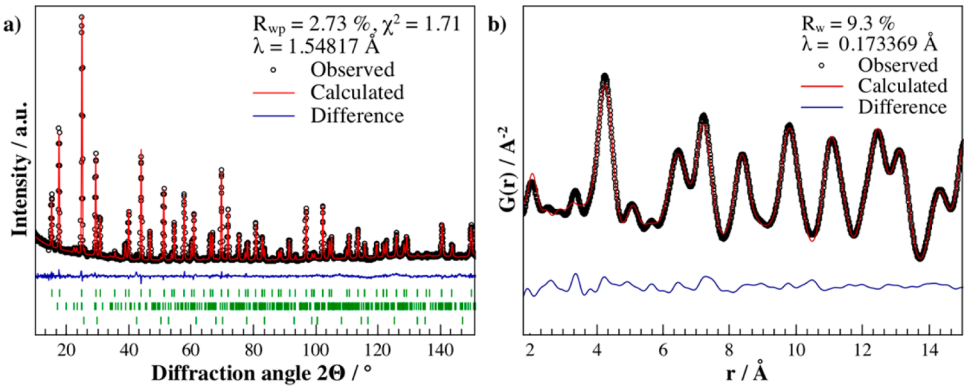

Figure 2. (a) Neutron powder diffraction data and results of the Rietveld refinement for Li_6PS_5I as a representative refinement. Small fractions of the impurity phases Li_3PO_4 and LiI can be seen and correspond to 1.5 and 1.6 wt %, respectively. (b) Pair distribution function [$G(r)$] of Li_6PS_5I, showing the goodness-of-fit of the structural refinement. An additional distance contribution around 3.4 Å can be seen that cannot be explained by the structural motif and appears to be decreasing from Cl to I.

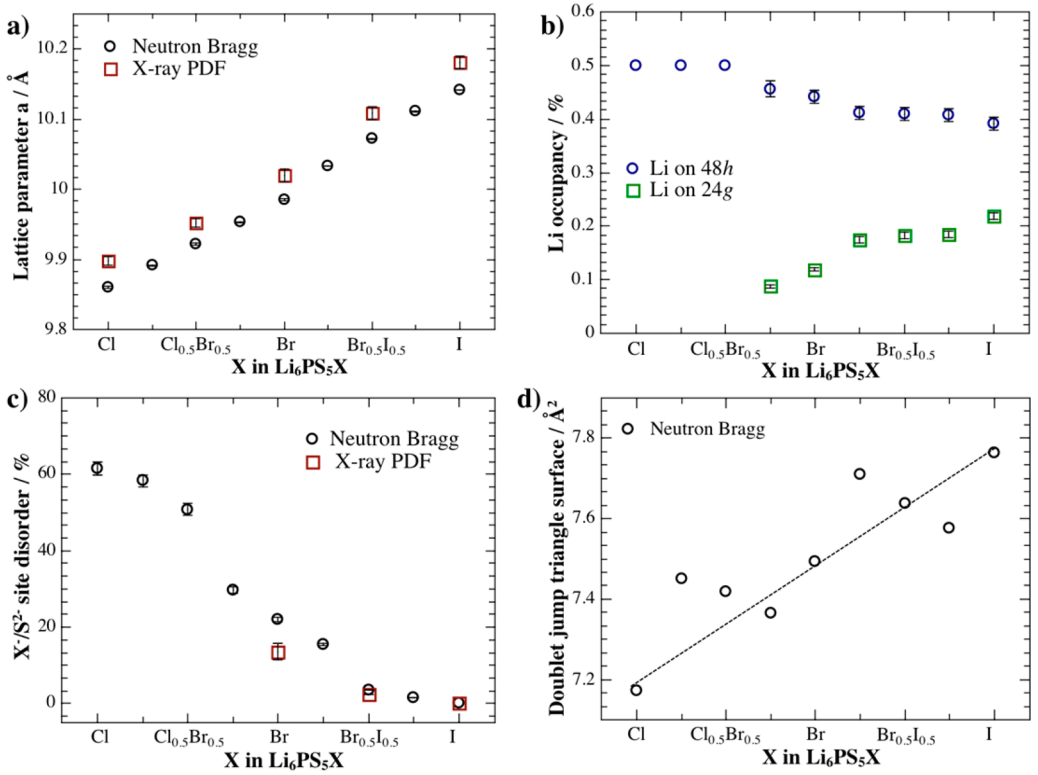

Figure 3. Structural data of Li_6PS_5X obtained from the Rietveld refinements of neutron powder diffraction data and X-ray pair distribution function analysis. (a) Increasing lattice parameters due to the increasing ionic radii of the halide anions. (b) With increasing unit cell volume, the Li occupancies change and a higher volume stabilizes Li in the transition state Wyckoff position 24*g*. (c) Observed site disorder between the halides and sulfur anions on the 4*c* site, which decreases with increasing anion radius. (d) Surface area of the triangle site for the 48*h*−24*g*−48*h* jump. The area increases, which stabilizes the occupancy of Li on the transition state site.

$$v_D = \left(\frac{3}{4\pi V}\right)^{1/3} v_{mean} \quad (4)$$

These equations show that a decreasing speed of sound directly relates to a decreasing Debye temperature and Debye frequency, which are parameters that reflect the phonon vibrational frequencies of a material.

3. RESULTS

Structural Characterization. The Li^+ superionic argyrodites Li_6PS_5X have been synthesized with various ratios of X (X = Cl, $Cl_{0.75}Br_{0.25}$, $Cl_{0.5}Br_{0.5}$, $Cl_{0.25}Br_{0.75}$, Br, $Br_{0.75}I_{0.25}$, $Br_{0.5}I_{0.5}$, $Br_{0.25}I_{0.75}$, and I) to study the effect of the anion polarizability on the lattice stiffness and the associated ionic conductivity. The substitution of X in Li_6PS_5X only changes the polarizability and lattice parameter of the anion sublattice, without significantly changing the conduction pathways or altering the charge carrier concentration, thereby making the Li^+ superionic argyrodites an ideal model system. This class of materials has been well-studied in efforts to elucidate Li^+ conducting phases and their conduction mechanisms, for instance by Deiseroth et al.,[61−63] and are, therefore, a good starting point for studying lattice dynamics effects. It should also be noted that the Ag and Cu superionic compounds exist as well. Figure 1a shows the

DOI: 10.1021/jacs.7b06327
J. Am. Chem. Soc. 2017, 139, 10909−10918

unit cell of Li_6PS_5X, in which the X^- anions form a face-centered cubic lattice (Wyckoff positions 4*a* and 4*c*), with S^{2-} anions in half of the tetrahedral voids and PS_4^{3-} tetrahedra on the octahedral sites (P on Wyckoff 4*b*). The I^- and S^{2-} anions are known to be separated between the different crystallographic sites, 4*a* and 4*c*, respectively. However, the Br^-- and Cl^--containing compounds are supposed to show significant site disorder.[63] The disorder, which has been shown experimentally for Li_6PS_5Cl and Li_6PS_5Br,[64−66] is very likely due to the similar ionic radii of Cl^- (1.81 pm), Br^- (1.96 pm), and S^{2-} (1.84 pm).[63,67]

With regard to the lithium ions, two crystallographic positions for Li^+ are possible[61] (Wyckoff 48*h* and 24*g*), of which the 24*g* site represents an intermediate state with triangular coordination through which diffusion can occur. The two lithium positions form cagelike local polyhedra (Figure 1b), where three different Li^+ jump processes are possible.[64,68] These include next-neighbor jumps (48*h*−24*g*−48*h*), intracage jumps, and intercage jumps, the latter of which seem to dominate the macroscopic long-range ion transport.[64] The occurring site disorder affects the intercage jumps and long-range transport. For example, I^--containing samples without any disorder exhibit higher activation barriers for conduction.[64,65] A high site disorder seems to be beneficial for the jump rate of the intercage jump.[64] This is possibly due to the more directional covalent character of the S^{2-} anion, which leads to a large degree of fluctuating chemical environments.[69]

Figure 2a shows a representative Rietveld refinement against neutron powder diffraction data, which has been collected for all samples in the series of solid solutions. In addition, X-ray pair distribution function (PDF) analysis of samples with 0.5 steps of halide content were also collected (see Figure 2b). The PDF were obtained to determine if local structural changes are induced by the substitution. All samples exhibit minor impurities (phase fraction below 5 wt %) of Li_3PO_4 and LiX, and the obtained structural data is tabulated in the Supporting Information. While no large local structural changes can be seen in the PDF, an additional distance arises around 3.4 Å that does not correspond to any local distances in the structure of Li_6PS_5X and seems to be decreasing from Cl to I (see the Supporting Information). For instance, in Li_6PS_5Br, the local distances are d(P−S) = 2.054(9) Å, d(S−S) = 3.35(1) Å (within a PS_4^{3-} unit), and d(S−S) = 3.73(2) Å (between two PS_4^{3-} units). All other S−X distances are greater than 4 Å. Presently, we believe that this may be due to some additional glassy phase, as recently shown in $Li_4P_2S_6$,[70] an assumption that is corroborated by the changing amorphous signals in ^{31}P NMR reported by Deiseroth and co-workers.[63]

Figure 3 shows all structural data obtained from refinements against the neutron diffraction data and the X-ray PDF, whenever applicable. All refined structural data can further be found tabulated in the Supporting Information. The linear increase in the lattice parameters due to the increasing anion radius follows Vegard's law, indicating the successful synthesis of all solid solutions in Li_6PS_5X (Figure 3a). Due to the time- and space-averaging character of the Bragg data, the lattice parameters, as obtained from PDF and neutron Bragg scattering data, deviate slightly. With the strong negative nuclear scattering form factor of Li, lithium occupancies on the two sites (i.e., 48*h* and 24*g*) are also obtained from the refinements (see Figure 3b). At high Cl content, no Li can be identified on the 24*g* position (the central position of the triangular site shown in Figure 1b). In other words, a 50% occupancy on the 48*h* site suggests that every next-neighbor Li site in the cage is unoccupied on average. With increasing Br and I substitution, the Li occupancy of the 48h site decreases, while it increases on the 24*g* one. The occupancy on the 24*g* site can be explained structurally. Figure 3d shows the surface area of the triangle sites for the jump from 48*h* to 24*g* to 48*h*, in which the 24*g* position represents the transition state on the triangular site. With increasing lattice volume, the distance between Li and S (on Wyckoff 16*e* and 4*c*, respectively) increases, which stabilizes the occupation of the transition state. Figure 4 shows the changing Li^+−Li^+ jump distances. With increasing unit cell volume, the intra- and intercage jump distances increase, while the 48*h*−48*h* separation decreases.

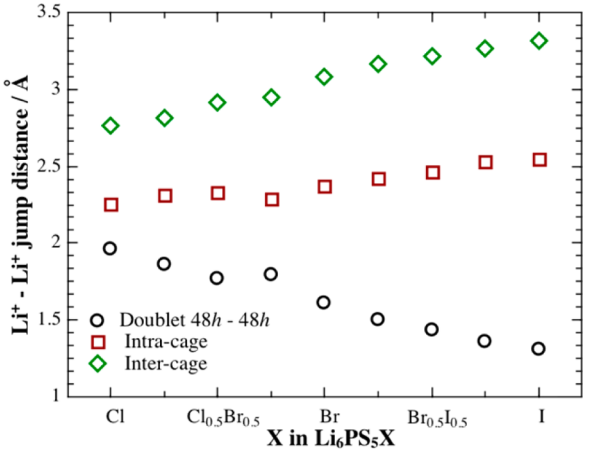

Figure 4. Li^+−Li^+ jump distances in Li_6PS_5X obtained from the Rietveld refinements of neutron powder Bragg data. With increasing unit cell volume, the intra- and intercage jump distances increase, while the doublet distance decreases, possibly due to being a measure of the Li^+ disorder.

Figure 3c shows the obtained site disorder between X and S on Wyckoff position 4*c* in which the percentage of shown disorder represents the total fraction of all X^- on the S^{2-} site. The individual occupancies of Cl, Br, and I can be found in the Supporting Information. The X-ray PDF data for Cl^--containing samples were not refined for disorder, as Cl^- and S^{2-} are indistinguishable via X-ray diffraction. In accordance with the literature,[63] significant site disorder between Cl^-, as well as Br^- and S^{2-}, is observed. With increasing lattice volume, and an increasing difference in the ionic radius variation of the anions, the site disorder decreases. No disorder is observable for Li_6PS_5I, as the ionic radii of I^- and S^{2-} are too different.

The change from Cl to Br and then to I leads to a clear change in the volume of the lattice, as well as the site disorder. The diminishing disorder is expected to increase the activation barrier of the observable transport.[64] In addition, these data show that with increasing lattice size, the probability of finding Li^+ on the transition state site 24*g* increases, which may ultimately affect the ionic transport, given that the lifetime of the excited transition state is clearly increasing. While changes in the structure are clearly visible, these effects are not expected to have a major influence on the diffusion pathways per se, as they do not alter the routes of Li diffusion in the structure.

Correlation of a Soft Lattice with Ionic Transport. In order to correlate changes of the ionic conductivity with lattice softness, temperature-dependent impedance spectroscopy was performed. The temperature dependence of the ionic

DOI: 10.1021/jacs.7b06327
J. Am. Chem. Soc. 2017, 139, 10909−10918

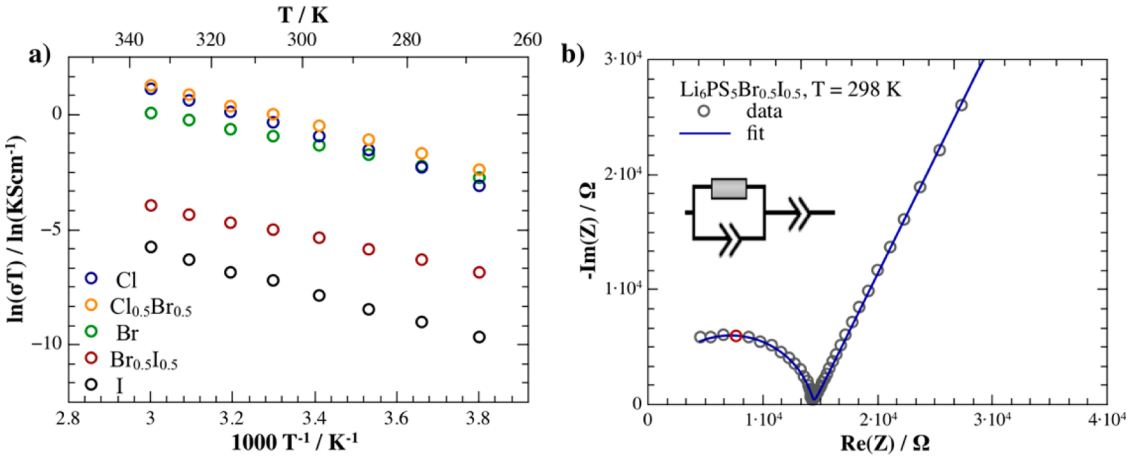

Figure 5. (a) Representative Arrhenius plots of Li_6PS_5X, in 0.5 steps for clarity, obtained via temperature-dependent impedance spectroscopy. (b) Selected Nyquist plot of $Li_6PS_5Br_{0.5}I_{0.5}$ showing the quality of the impedance data and the fit with the shown equivalent circuit. The apex frequency corresponds to 1.1×10^6 Hz and is shown as a red data point.

conductivity is often given as an Arrhenius-equivalent process:[71]

$$\sigma T = \sigma_0 \exp\left(-\frac{E_A}{k_B T}\right) \quad (5)$$

with the activation energy being E_A and the prefactor being σ_0. The temperature-dependent ionic conductivity of Li_6PS_5X was measured using impedance spectroscopy, and the resulting Arrhenius plots (shown in 0.5 steps for clarity) are shown in Figure 5a, with a representative impedance response for $Li_6PS_5Br_{0.5}I_{0.5}$ shown in Figure 5b. The extracted activation barriers for ionic motion are shown in Figure 6b and are discussed in the context of the varying lattice stiffness (vide infra). The impedance data were fit to an equivalent circuit consisting of one parallel CPE/resistor in series with a CPE representing the blocking electrodes. The apex frequency is 1.1×10^6 Hz, which corresponds to a capacitance of 1.2×10^{-9} F. Bulk and grain boundary contributions cannot be deconvoluted and the conductivities reported correspond to the overall sample conductivity. While the mechanistic considerations relate to the bulk transport, it is reasonable to assume that the grain boundary contributions do not significantly affect the observed trends, as the standard deviations obtained will reflect spreads in sample density as well.

Ultrasonic determination of the stiffness of a material can be performed by (1) directly measuring the speed of sound using a pulse-echo method or (2) measuring the resonant vibrational frequencies of the sample (resonant ultrasound spectroscopy, RUS).[51−53] In both cases, for a sample of known density and dimensions, the elastic constants and the transverse and longitudinal sound velocities can be determined with a high degree of accuracy. In the present study, both methods were used to independently confirm the trend in the velocity as a function of composition. In addition to providing information about the bond strength and elastic constants of a material,[72] the measured speeds of sound determine the slope of the acoustic phonon branches and are, therefore, a good and reliable measure of phononic properties and lattice stiffness. A high speed of sound, which directly indicates a more rigid lattice with stiffer bonds (reduced spring constant), corresponds to high Debye temperatures and high Debye frequencies (see eqs 3 and 4).[54] Ultrasonic speed of sound measurements have been used previously to obtain elastic constants of lithium conducting thiophosphates[73−75] and, just recently, the Debye temperature of $Li_{10}GeP_2S_{12}$.[50] Baranowski et al.[73] found that speed of sound measurements (which are generally considered to be more accurate than indentation)[51−53] correlate well with indentation experiments, if the density of the samples is considered.

Figure 6 shows the obtained speeds of sound (longitudinal, transverse, and mean speeds), the linear-fit extracted activation barriers, the Arrhenius prefactors, and the room-temperature ionic conductivities for all compositions of Li_6PS_5X. In order to account for variations in the microstructure, density, and syntheses, three different samples were synthesized and measured for each composition. Despite increasing the lattice volume and anion polarizability, the speeds of sound decrease (Figure 6a), corresponding to an increase in the softness of the lattice and, with it, decreasing Debye temperatures and Debye frequencies of the solids (vide infra). Although slightly higher speeds of sound would be expected for fully dense samples,[73] the qualitative trend reflects the softening of the lattice when substituting Cl for Br and I.

The linear-fit extracted E_A and prefactors σ_0 for the different materials can be found in Figure 6b. It is evident that the substitution of heavier halide anions leads to a decrease in the activation barrier and a decrease in the prefactor σ_0, as expected within the Meyer−Neldel rule,[76−80] with the exception of the iodine-containing Li_6PS_5X. Here, the absence of site disorder leads to an increasing activation barrier, as expected from theoretical considerations.[64] The decrease of the activation barrier and the prefactor σ_0 correlates well with the increasing softness of the lattice (Figure 6a). The concurrent decrease of both variables in eq 5, i.e., the Arrhenius prefactor σ_0 and the activation barrier E_A, leads to an optimum of the ionic conductivity at a composition of $Li_6PS_5Cl_{0.5}Br_{0.5}$. These data demonstrate an experimental correlation between the softness of a lattice and the activation barrier in ionic conductors. However, with decreasing lattice softness, the Arrhenius prefactor is strongly influenced, which in turn detrimentally affects the ionic conductivity.

4. DISCUSSION

The collected data provide evidence that a correlation indeed exists between a softer lattice and the ionic transport. With

DOI: 10.1021/jacs.7b06327
J. Am. Chem. Soc. 2017, 139, 10909−10918

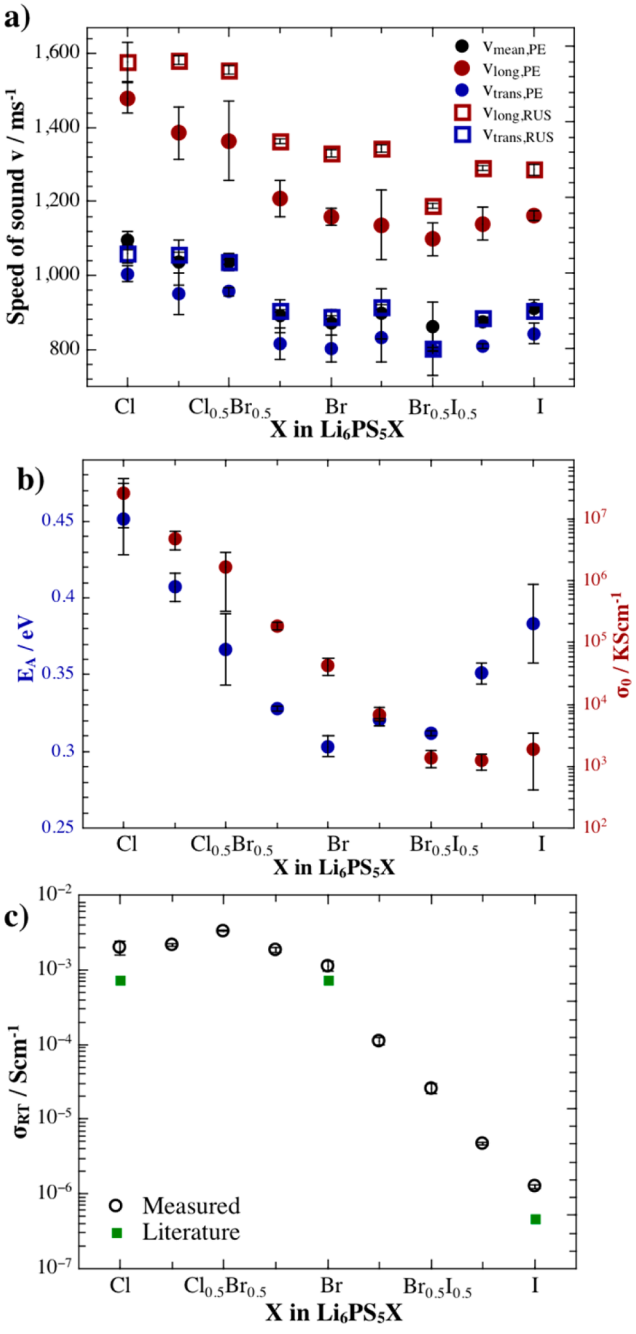

Figure 6. (a) Measured speeds of sound for Li_6PS_5X using the sound-response echo method (PE) and resonant ultrasound spectroscopy (RUS). With increasing polarizability of the halide anion, the speed of sound decreases and then slightly increases for Li_6PS_5I. (b) With decreasing lattice stiffness (i.e., decreasing speed of sound), the activation energy and the prefactor σ_0 decrease. The increase in the iodine-containing samples can be attributed to the lack of anion disorder. The concurrent decrease of E_A and σ_0 leads to an overall decrease of the (c) conductivity with increasing softness of the anion lattice. The decrease of E_A, as well as σ_0, due to a softening of the lattice suggests an optimal lattice softness in ionic conductors for maximum conductivity. The literature values are shown for comparison.[66] All error bars represent standard deviations obtained from measurements on three samples per composition.

increasing lattice softness, i.e., weaker bonds and decreasing speeds of sound, the Arrhenius prefactor σ_0 and the activation barrier E_A decrease. The decreasing activation barrier with lattice softening and lower phonon frequencies has been discussed in the literature;[41,81,82] however, the effect of a softer lattice on the Arrhenius prefactor has so far been overlooked and leads to a decreasing conductivity of solid electrolytes with very soft lattices.

Within the framework of the conventional hopping theory, the prefactor σ_0 is given by[71]

$$\sigma_0 = \frac{zn(\mathrm{Ze})^2}{k_B} e^{\Delta S_m/k_B} a_0^2 \nu_0 \quad (6)$$

governed by a factor to take into account different diffusion geometries and correlation factors (z), the carrier density of mobile ions (n), the entropy of migration (ΔS_m), the jump distance (a_0), the charge of the ions (Ze), and the attempt frequency (ν_0). The attempt frequency corresponds to the oscillator frequency of a moving cation on its lattice site and can, in terms of a transition state theory, be described as the inverse of the lifetime of the excited ion state.[32] The frequency of the occurring jump (jump frequency) then is a product of the probability of the occurring jump and the attempt frequency.[71] The migration enthalpy is related to that soft vibrational mode that carries the ion across the saddle point[83,84] and, hence, the attempt frequency. The entropy of migration itself also depends on the phonon properties, as it is directly related to the ratio of the vibrational partition functions of the excited and the initial state.[83,85] In other words, both the migrational entropy as well as the enthalpy, i.e., the activation energy, are directly affected by the lattice vibrations. In this work, changing the anion isoelectronically does not change the number of charge carriers nor the diffusion pathways or the defect formation enthalpies. The increasing anion size increases the jump distance (see Figure 4) and the increasing polarizability induces a softening of the lattice (Figure 6a). This leads to lower speeds of sound, lower Debye temperatures, and lower Debye frequencies (see eqs 3 and 4). The Debye frequencies (ν_D), as obtained from the mean speeds of sound, for the different compositions are shown in Figure 7a and decrease as the lattice becomes softer. Since the attempt frequency (ν_0) is usually approximated using the Debye frequency (ν_D),[86,87] a softening of the lattice should lead to a decrease in the prefactor. Using the formalism of transition state theory of ionic motion, the oscillator frequency can be estimated from the activation barrier via[32]

$$\nu_0 = \frac{1}{a_0}\sqrt{\frac{2E_A}{M_{Li}}} \quad (7)$$

Figure 7b shows the jump frequency (ν_0) versus the Debye frequency (ν_D) of the different compositions, calculated via eq 7 from the measured activation barriers, as well as the jump distance of the intercage jump (Figure 4). A direct correlation can be seen, within the estimated errors obtained by propagation of the standard deviations, in that the activation barriers are influenced by a softening of the lattice. The influence of the lattice vibrations on the prefactor and the activation barrier may indeed be one explanation for the origin of the Meyer–Neldel rule (or compensation rule),[76−80] which states that a decreasing activation barrier often coincides with a lower prefactor. It should be noted, however, that the Debye frequencies as obtained from pulse-echo measurements are an order of magnitude smaller than the obtained frequencies. Some of the deviation may be due to the lower density of the samples[73] or the used intracage jump distances, which may not

DOI: 10.1021/jacs.7b06327
J. Am. Chem. Soc. 2017, 139, 10909−10918

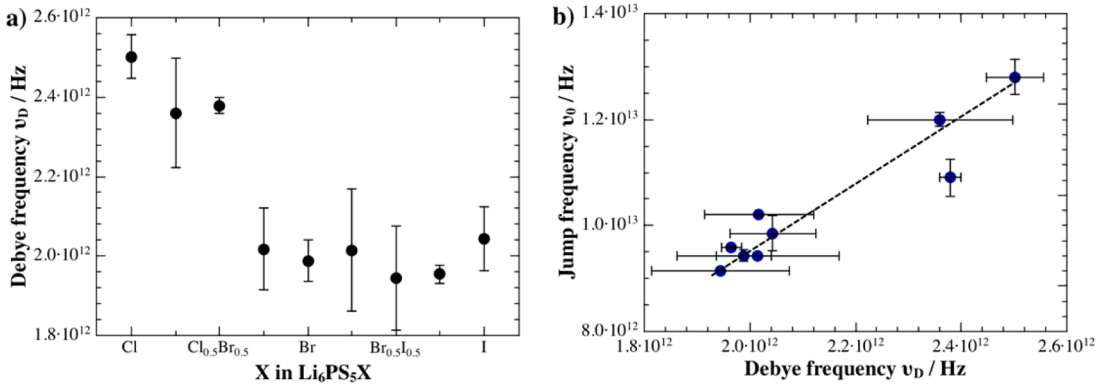

Figure 7. (a) Debye frequencies in the series of Li_6PS_5X solid solutions. With increasing polarizability of the halide anion, the Debye frequency decreases. (b) Jump frequencies as obtained from the measured activation barriers and crystallographic jump distances against the obtained Debye frequencies. A correlation exists (dashed line as a guide-to-the-eye), linking the lattice softness and Debye frequency to the jump frequency of a moving ion.

reflect the rate-limiting jump for long-range transport. It shows that the typical approximation of $\nu_D = \nu_0$ is not entirely correct, as it is solely based on a parabolic potential well. Furthermore, with the changing site disorder, the predominant jump process may change, which would further affect the overall jump frequency and prefactor. In addition, diffusion in the solid state is, in general, a many-body problem. Depending on the exact local bonding, the herein extracted Debye frequencies and measured speeds of sound represent an average over all chemical bonding interactions present in Li_6PS_5X. In other words, averaging of the more ionic Li^+−anion bonding and the covalent P−S interactions may lead to further deviations in the average Debye frequency relative to the jump frequency of Li^+ in its anion framework.

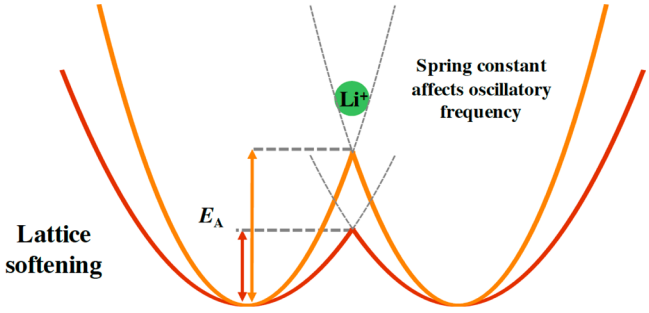

Figure 8. Schematic of the effect of lattice softening on the ion jump. With increasing lattice softness, i.e., changing bond strength, the local jump oscillators broaden, thereby altering the vibrational frequency, as well as the activation barrier for a jump.

Figure 7b shows that with decreasing lattice softness, the activation barrier and Debye frequency, as well as the attempt frequency of ionic motion, decrease (see Figure 8). However, the experimentally determined prefactor (see Figure 6b) changes much faster and over orders of magnitude compared to the changing jump frequency. At this stage, we assume that the changing vibrational frequencies of the lattice affects the entropy of migration more strongly through the ratio of the vibronic partition functions. Furthermore, while the site disorder in the I-containing material leads to an increase in the activation barrier, the prefactor continues to decrease (see the Supporting Information, Figure S2). This shows that while local structural changes affect the activation energy as well, the entropy of migration is only dependent on the lattice vibrations.

The lattice softening leads to a lower Debye frequency, which lowers the jump frequency, and the entropy of migration. All of these decrease the Arrhenius prefactor as well the activation barrier for the ion jump (Figure 8). Interestingly, the decreasing jump frequency should lead to an increased lifetime (τ_0) of the excited state ($\nu_0 = 1/\tau_0$),[32] and indeed, the occupancy of the 24*g* position increases along the solid solutions series (see Figure 3b). Whether the increasing population of the 24*g* position, and increasing lifetime of this transition site, derives from a larger lattice (i.e., more space for occupation) or whether it is due to a softer lattice remains unclear at this stage.

The observed correlation between a softer lattice and the oscillator frequency of a moving ion shows that a softer lattice indeed lowers the activation barrier, as assumed in the past, but also affects the Arrhenius prefactor, leading to an optimum lattice softness for $Li_6PS_5Cl_{0.5}Br_{0.5}$ and a rapid decrease in the conductivity for lattices that are too soft. In addition, these data experimentally confirm the theoretical proposition[64] that a decreasing site disorder increases the activation barrier for a jump, which explains the low conductivities in the iodine-containing argyrodites when taking the Arrhenius prefactor into consideration.

5. CONCLUSION

In this work, the effect of lattice polarizability on the ionic conductivity has been studied in the Li_6PS_5X argyrodites. Using a combination of neutron diffraction and synchrotron pair-distribution function analysis, lattice variations and, more specifically, the Li^+ occupancies and X^-/S^{2-} site disorder were monitored. In addition, speeds of sound measurements were used to obtain information about changes in the lattice softness, upon substituting the anion sublattice from rigid Cl^- to the more polarizable I^-.

Impedance spectroscopy showed that changing the lattice dynamics (in this case by softening the lattice) affects ionic motion within solids. A softer lattice lowers the migration barrier for a moving cation, as previously proposed, but this work further demonstrates that the softer lattice affects both the oscillator frequency of a moving ion and the Arrhenius prefactor as well. This suggests that the commonly accepted paradigm of "a softer lattice for higher conductivities" may not

DOI: 10.1021/jacs.7b06327
J. Am. Chem. Soc. 2017, 139, 10909−10918

be as straightforward as previously thought. These data show the first systematic study of the effects of lattice softening on ionic conduction within one material class. This may provide a novel optimization approach in the field of ionic conductors, and more importantly, it shows that a deeper understanding of the effects of a dynamic lattice on the jump frequencies, and ultimately the ionic transport, is still required.

■ ASSOCIATED CONTENT

Supporting Information

The Supporting Information is available free of charge on the ACS Publications website at DOI: 10.1021/jacs.7b06327.

All structural data as obtained from Rietveld refinements against neutron Bragg data can be found here, as well as the pair distribution functions for the different argyrodites and a Meyer−Neldel plot (PDF)

■ AUTHOR INFORMATION

Corresponding Author

*wolfgang.g.zeier@phys.chemie.uni-giessen.de

ORCID

Alexandra Zevalkink: 0000-0002-4672-7438

Wolfgang G. Zeier: 0000-0001-7749-5089

Notes

The authors declare no competing financial interest.

■ ACKNOWLEDGMENTS

This work was supported by Diamond Light Source (beamtime awards EE13560) with beamtime proposal SP13560. W.G.Z furthermore gratefully acknowledges the financial support through start-up funding provided by the Justus-Liebig-University Giessen. The authors thank Dr. Kai Weldert and Dr. Dominik Weber for valuable discussions.

■ REFERENCES

(1) Tarascon, J.-M.; Armand, M. *Nature* **2001**, *414*, 359.
(2) Goodenough, J. B.; Park, K.-S. *J. Am. Chem. Soc.* **2013**, *135* (4), 1167.
(3) Janek, J.; Zeier, W. G. *Nat. Energy* **2016**, *1*, 16141.
(4) Goodenough, J. B. *Solid State Ionics* **1997**, *94*, 17.
(5) Chueh, W. C.; Falter, C.; Abbott, M.; Scipio, D.; Furler, P.; Haile, S. M.; Steinfeld, A. *Science (Washington, DC, U. S.)* **2010**, *330*, 1797.
(6) West, A. R. *Basic Solid State Chemistry*, 2nd ed.; John Wiley & Sons: West Sussex, England, 2008.
(7) Boyce, J. B.; Huberman, B. A. *Phys. Rep.* **1979**, *51* (4), 189.
(8) Sato, H. In *Solid Electrolytes*; Geller, S., Ed.; Springer Verlag: Berlin, 1977; pp 3−39.
(9) Nilges, T.; Pfitzner, A. *Z. Kristallogr. - Cryst. Mater.* **2005**, *220*, 281.
(10) Gaudin, E.; Petricek, V.; Boucher, F.; Taulelle, F.; Evain, M. *Acta Crystallogr., Sect. B: Struct. Sci.* **2000**, *56* (6), 972.
(11) Thangadurai, V.; Kaack, H.; Weppner, W. *J. Am. Ceram. Soc.* **2003**, *86*, 437.
(12) Cussen, E. J. *Chem. Commun.* **2006**, 412.
(13) Wang, Y.; Richards, W. D.; Ong, S. P.; Miara, L. J.; Kim, J. C.; Mo, Y.; Ceder, G. *Nat. Mater.* **2015**, *14* (10), 1026.
(14) Urban, A.; Lee, J.; Ceder, G. *Adv. Energy Mater.* **2014**, *4*, 1400478.
(15) Wang, Y.; Richards, W. D.; Ong, S. P.; Miara, L. J.; Kim, J. C.; Mo, Y.; Ceder, G. *Nat. Mater.* **2015**, *14*, 1026.
(16) Mahan, G. D. In *Superionic Conductors*; Mahan, G. D., Ed.; Springer, 1976; pp 115−134.
(17) Zeier, W. G.; Zhou, S.; Lopez-Bermudez, B.; Page, K.; Melot, B. C. *ACS Appl. Mater. Interfaces* **2014**, *6* (14), 10900.
(18) Kamaya, N.; Homma, K.; Yamakawa, Y.; Hirayama, M.; Kanno, R.; Yonemura, M.; Kamiyama, T.; Kato, Y.; Hama, S.; Kawamoto, K.; Mitsui, A. *Nat. Mater.* **2011**, *10* (9), 682.
(19) Bron, P.; Johansson, S.; Zick, K.; Schmedt auf der Günne, J.; Dehnen, S.; Roling, B. *J. Am. Chem. Soc.* **2013**, *135* (42), 15694.
(20) Kanno, R.; Hata, T.; Kawamoto, Y.; Irie, M. *Solid State Ionics* **2000**, *130* (1), 97.
(21) Muruyama, M.; Kanno, R.; Irie, M.; Ito, S.; Hata, T.; Sonoyama, N.; Kawamoto, Y. *J. Solid State Chem.* **2002**, *168*, 140.
(22) Zeller, H. R.; Brüesch, P.; Pietronero, L.; Strässler, S. In *Superionic Conductors*; Mahan, G. D., Ed.; Springer, 1976; pp 201−214.
(23) Knauth, P. *Solid State Ionics* **2009**, *180* (14−16), 911.
(24) Rangasamy, E.; Liu, Z.; Gobet, M.; Pilar, K.; Sahu, G.; Zhou, W.; Wu, H.; Greenbaum, S.; Liang, C. *J. Am. Chem. Soc.* **2015**, *137* (4), 1384.
(25) Sen, P. N.; Huberman, B. A. *Phys. Rev. Lett.* **1975**, *34*, 1059.
(26) Huberman, B. A.; Sen, P. N. *Phys. Rev. Lett.* **1974**, *33*, 1379.
(27) Allen, S. J.; Remeika, J. P. *Phys. Rev. Lett.* **1974**, *33*, 1478.
(28) Pardee, W. J.; Mahan, G. D. *J. Solid State Chem.* **1975**, *15*, 310.
(29) Bührer, W.; Nicklow, R. M.; Brüesch, P. *Phys. Rev. B: Condens. Matter Mater. Phys.* **1978**, *17* (8), 3362.
(30) Fischer, K.; Bilz, H.; Haberkorn, R.; Weber, W. *Phys. Status Solidi B* **1972**, *54*, 285.
(31) Brüesch, P.; Pietronero, L.; Strässler, S.; Zeller, H. R. *Phys. Rev. B* **1977**, *15* (10), 4631.
(32) Rice, M. J.; Roth, W. L. *J. Solid State Chem.* **1972**, *4*, 294.
(33) Ebbsjö, I.; Vashishta, P.; Dejus, R.; Sköld, K. *J. Phys. C: Solid State Phys.* **1987**, *20*, L441.
(34) Schmalzl, K.; Strauch, D.; Schober, H. *Phys. Rev. B: Condens. Matter Mater. Phys.* **2003**, *68* (14), 144301.
(35) Alben, R.; Burns, G. *Phys. Rev. B* **1977**, *16* (8), 3746.
(36) Ghosh, S.; Chatterjee, S.; Basu, A. N. *Phys. Status Solidi B* **1984**, *123* (2), 445.
(37) Samara, A. *Ferroelectrics* **1977**, *17*, 357.
(38) Gopal, C. B.; van de Walle, A. *Phys. Rev. B: Condens. Matter Mater. Phys.* **2012**, *86*, 134117.
(39) Li, X.; Benedek, N. A. *Chem. Mater.* **2015**, *27* (7), 2647.
(40) Jansen, M. *Angew. Chem., Int. Ed. Engl.* **1991**, *30* (12), 1547.
(41) Bachman, J. C.; Muy, S.; Grimaud, A.; Chang, H. H.; Pour, N.; Lux, S. F.; Paschos, O.; Maglia, F.; Lupart, S.; Lamp, P.; Giordano, L.; Shao-Horn, Y. *Chem. Rev.* **2016**, *116* (1), 140.
(42) Hoelzel, M.; Senyshyn, A.; Dolotko, O. *J. Large-Scale Res. Facil. JLSRF* **2015**, *1*, A5.
(43) Hoelzel, M.; Senyshyn, A.; Juenke, N.; Boysen, H.; Schmahl, W.; Fuess, H. *Nucl. Instrum. Methods Phys. Res., Sect. A* **2012**, *667*, 32.
(44) Toby, B. H.; Von Dreele, R. B. *J. Appl. Crystallogr.* **2013**, *46*, 544.
(45) Young, R. A. *The Rietveld Method*; Oxford University Press: New York, 1993.
(46) Thompson, P.; Cox, D. E.; Hastings, J. B. *J. Appl. Crystallogr.* **1987**, *20* (2), 79.
(47) Qiu, X.; Thompson, J. W.; Billinge, S. J. L. *J. Appl. Crystallogr.* **2004**, *37* (4), 678.
(48) Farrow, C. L.; Juhas, P.; Liu, J. W.; Bryndin, D.; Božin, E. S.; Bloch, J.; Proffen, T.; Billinge, S. J. L. *J. Phys.: Condens. Matter* **2007**, *19* (33), 335219.
(49) Petkov, V.; Gateshki, M.; Niederberger, M.; Ren, Y. *Chem. Mater.* **2006**, *3* (5), 814.
(50) Weber, D. A.; Senyshyn, A.; Weldert, K. S.; Wenzel, S.; Zhang, W.; Kaiser, R.; Berendts, S.; Janek, J.; Zeier, W. G. *Chem. Mater.* **2016**, *28*, 5905−5915.
(51) Leisure, R. G.; Willis, F. A. *J. Phys.: Condens. Matter* **1997**, *9*, 6001.
(52) Zadler, B. J.; Le Rousseau, H. L.; Scales, J. A.; Smith, M. L. *Geophys. J. Int.* **2004**, *156*, 154.
(53) Alberts, H. L. *Encycl. Mater. Sci. Technol.* **2002**, 1.
(54) Zeier, W. G.; Zevalkink, A.; Gibbs, Z. M.; Hautier, G.; Kanatzidis, M. G.; Snyder, G. J. *Angew. Chem., Int. Ed.* **2016**, *55* (24), 6826.

(55) Heinrich, C. P.; Day, T. W.; Zeier, W. G.; Snyder, G. J.; Tremel, W. *J. Am. Chem. Soc.* **2014**, *136*, 442.
(56) Weldert, K. S.; Zeier, W. G.; Day, T. W.; Panthöfer, M.; Snyder, G. J.; Tremel, W. *J. Am. Chem. Soc.* **2014**, *136*, 12035.
(57) Toberer, E. S.; Zevalkink, A.; Snyder, G. J. *J. Mater. Chem.* **2011**, *21*, 15843.
(58) May, A. F.; Snyder, G. J. In *Thermoelectrics Handbook: Thermoelectrics and Its Energy Harvesting*; Rowe, D. M., Ed.; CRC Press: Boca Raton, FL, 2012.
(59) Zevalkink, A.; Toberer, E. S.; Zeier, W. G.; Flage-Larsen, E.; Snyder, G. J. *Energy Environ. Sci.* **2011**, *4* (2), 510.
(60) Anderson, O. L. *J. Phys. Chem. Solids* **1963**, *24*, 909.
(61) Kong, S. T.; Gün, O.; Koch, B.; Deiseroth, H. J.; Eckert, H.; Reiner, C. *Chem. - Eur. J.* **2010**, *16* (17), 5138.
(62) Deiseroth, H.; Maier, J.; Weichert, K.; Nickel, V.; Kong, S.; Reiner, C. *Z. Anorg. Allg. Chem.* **2011**, *637*, 1287.
(63) Deiseroth, H. J.; Kong, S. T.; Eckert, H.; Vannahme, J.; Reiner, C.; Zaiß, T.; Schlosser, M. *Angew. Chem., Int. Ed.* **2008**, *47* (4), 755.
(64) de Klerk, N. J. J.; Rosłoń, I.; Wagemaker, M. *Chem. Mater.* **2016**, *28*, 7955.
(65) Chen, H. M.; Maohua, C.; Adams, S. *Phys. Chem. Chem. Phys.* **2015**, *17* (25), 16494.
(66) Rayavarapu, P. R.; Sharma, N.; Peterson, V. K.; Adams, S. *J. Solid State Electrochem.* **2012**, *16* (5), 1807.
(67) Shannon, R. D. *Acta Crystallogr., Sect. A: Cryst. Phys., Diffr., Theor. Gen. Crystallogr.* **1976**, *A32*, 751.
(68) Yu, C.; Ganapathy, S.; de Klerk, N. J. J.; Roslon, I.; van Eck, E. R. H.; Kentgens, A. P. M.; Wagemaker, M. *J. Am. Chem. Soc.* **2016**, *138*, 11192.
(69) Adelstein, N.; Wood, B. C. *Chem. Mater.* **2016**, *28* (20), 7218.
(70) Dietrich, C.; Sadowski, M.; Sicolo, S.; Weber, D. A.; Sedlmaier, S. J.; Weldert, K. S.; Indris, S.; Albe, K.; Janek, J.; Zeier, W. G. *Chem. Mater.* **2016**, *28* (23), 8764.
(71) Tilley, R. J. D. *Defects in Solids*, 10th ed.; Wiley VCH: Hoboken, NJ, 2008.
(72) Zeier, W. G.; Zevalkink, A.; Gibbs, Z. M.; Hautier, G.; Kanatzidis, M. G.; Snyder, G. J. *Angew. Chem., Int. Ed.* **2016**, *55* (24), 6826.
(73) Baranowski, L. L.; Heveran, C. M.; Ferguson, V. L.; Stoldt, C. R. *ACS Appl. Mater. Interfaces* **2016**, *8* (43), 29573.
(74) Sakuda, A.; Hayashi, A.; Takigawa, Y.; Higashi, K.; Tatsumisago, M. *J. Ceram. Soc. Jpn.* **2013**, *121* (11), 946.
(75) Sakuda, A.; Hayashi, A.; Tatsumisago, M. *Sci. Rep.* **2013**, *3*, 2261.
(76) Kreuer, K.-D.; Kohler, H.; Maier, J. In *High Conductivity Ionic Conductors: Recent Trends and Applications*; Takahash, T., Ed.; World Scientific, 1989; pp 242−279.
(77) Meyer, W.; Neldel, H. *Z. Technol. Phys.* **1937**, 588.
(78) Ngai, K. *Solid State Ionics* **1998**, *105*, 231.
(79) Nowick, A. S.; Lee, W. K.; Jain, H. *Solid State Ionics* **1988**, *28*−*30*, 89.
(80) Knödler, D.; Pendzig, P.; Dieterich, W. *Solid State Ionics* **1996**, *86*−*88*, 29.
(81) Wakamura, K. *Phys. Rev. B: Condens. Matter Mater. Phys.* **1997**, *56* (18), 11593.
(82) Ishzi, T. *Solid State Ionics* **1987**, *28*−*30*, 67.
(83) Vineyard, G. H. *J. Phys. Chem. Solids* **1957**, *3*, 121.
(84) Wert, C.; Zener, C. *Phys. Rev.* **1949**, *76* (8), 1169.
(85) Toyoura, K.; Koyama, Y.; Kuwabara, A.; Oba, F.; Tanaka, I. *Phys. Rev. B: Condens. Matter Mater. Phys.* **2008**, *78*, 214303.
(86) Mehrer, H. *Diffusion in Solids—Fundamentals, Methods, Materials, Diffusion-Controlled Processes*; Springer-Verlag: Berlin, 2007.
(87) Crawford, J. H.; Slifkin, L. M. *Point Defects in Solids*, 1st ed.; Springer, 1972.

DOI: 10.1021/jacs.7b06327
J. Am. Chem. Soc. 2017, 139, 10909−10918